Computer Assisted Mechanics and Engineering Sciences, 10: 353–368, 2003.

FEM analysis of strain distribution in tibia bone and relationship between strains and adaptation of bone tissue

Romuald Będziński, Krzysztof Ścigała
Experimental Mechanics and Biomechanics Division,
Institute of Machine Design and Operation
Wrocław University of Technology, Wrocław, Poland

(Received May 13, 2002)

The purpose of the research is the estimation of strain distribution in tibia bone. Resultant strain distribution constitutes necessary data for the calculations made in the process of simulation of bone tissue adaptation. Estimation of strain distribution in proximal part of tibia bone is made for different load conditions (including the one following total knee arthroplasty and a surgical correction of lower limb with the application of high tibial osteotomy). The model of tibia bone and soft tissues, prepared for finite element analysis, was made with the use of Ansys 5.6. The geometry of bone was estimated by 3-D digitalisation of a physical model of bone. Displacements distribution obtained from the simulation was compared with the measurements of the physical model of a knee joint. In the research the holographic interferometry method was applied. The results of this calculation are helpful in the estimation of boundary conditions for a simulation of bone tissue functional adaptation in the region of a knee joint. It has been found out that there are differences in strain distribution in different load conditions. However, the perfect agreement of experimental and numerical results for a simple static load indicates that the numerical model is valid for this simulation in a certain range of the applied load.

Keywords: tibia bone, bone tissue adaptation, high tibial osteotomy, knee joint arthroplasty

1. Introduction

The human knee joint follows the hip joint in the statistics on the number of alloplasties performed. However, if other corrective procedures such as sub- and supragenual osteotomies are taken into consideration, then the number of surgical interventions in the knee joint region is similar or even higher than in the hip joint. All these procedures are directly related to degenerative changes in the proximal epiphysis of tibial bone which occur in both spongy tissue and compact bone. Whereas the pathomechanism of the changes is not fully understood, it is a well known fact that most of them stem from stress shielding, i.e. the adaptation of bone tissue to the unphysiological state of loading of the knee joint.

A number of papers describe such changes, particularly in the case of varus or valgus deformity of the knee joint and the associated overloading of one of its compartments [2–4, 18]. The main pathological sign is a lateral shift of the knee joint's centre in relation to the mechanical axis of the lower limb [2, 3]. There are some additional symptoms, e.g. a change in the width of the space on one side of the joint and excessive distension of the articular capsule's ligaments and fibres in the other side. In an advanced stage of the deformation of the joint, X-ray pictures reveal changes in the density of the subcartilaginous layer of the overloaded compartment of the tibial bone epiphysis and changes in the shape of the epiphysis itself [18]. Depending on the advancement of the degenerative changes, such illnesses are treated by popliteal osteotomy [2–4] or by implanting a knee joint prosthesis [1, 2]. If surgical treatment is applied, especially alloplasty, complications – loading induced degenerative changes in the bone tissue – result [2, 3, 18]. The main symptoms of

the complications are: the formation of a layer of fibrous tissue around the endoprosthesis, changes in the radiological density of the spongy bone and the loosening and migration of the endoprosthesis tibial component [1].

It should be noted that most of the phenomena described above are closely linked with functional adaptation processes and the remodelling of internal bone tissue in reaction to changes in the loading of the bone. The adaptation of human body tissues in mechanical loading is a fact which has been known for a long time. Wolfe's papers [27] were the first attempt to describe this phenomenon mathematically. Today we know that remodelling processes are connected with the changes in the activity of osteoblasts and osteoclasts, i.e. changes in the balance between the continuous absorption and resorption of bone tissue [7, 17, 19]. Numerous experimental research has established that there is a relationship between the variable loading of the skeletal system and changes in the density and mechanical properties of bone tissue [6, 8, 12, 15, 24]. Beaupre [5] proved that there is a relationship between the rate of changes in bone density and the mechanical stimulus representing the history of bone tissue loading. Carter showed that the relationships can be used to simulate the adaptations in the mechanical properties of bone tissue in the proximal epiphysis of femoral bone [15, 16] as a result of hip joint loading during walking. In papers [7, 11–13, 21], changes in the density and mechanical properties of bone tissue are described as a response to changes in its state of strains, with an assumption that the change in the principal strains is proportional to that in the bone tissue density. The papers by Weinans [23, 26] point out that the change in the mechanical properties of bone tissue occur in response to signals of mechanical stimulus acting on the sensors located in it. In numerous works [14, 22, 25], attempts were made to simulate the adaptations in bone tissue caused by the introduction of implants.

It should be noted that so far, most of the research has concentrated on the remodelling of femur bone and lumbar spine vertebrae. Similarly, simulations of the introduction of an implant into a human skeletal system have focused mainly on stems of hip joint endoprostheses [22, 25] and fixators for long bone fractures [10, 20]. Relatively little is known about the remodelling of tibial bone in the course of its deformation and loosening of the knee joint endoprosthesis tibial component.

Especially nowadays, the new diagnostic tools (computer tomography, MRI) play a significant role in the identification of bone density and mechanical properties of bone tissue, including cases of bone diseases and adaptation after surgery intervention. First relationships of mechanical and radiological properties of bone become more quantitative than qualitative. Thanks to modern tools of computer analysis we are gaining the possibility to predict bone behaviour even in the case of a particular patient. However, the progress in the research on the relationships of mechanical and radiological properties of bone, as well as the development of new procedures of computer simulations, is necessary.

The main aim of this research work was to determine the distribution of strains in bone tissue under a knee joint loading and to simulate the adaptations in the mechanical properties and the density of bone tissue in the proximal epiphysis of tibial bone in reaction to changes in the loading, including changes due to varus deformity in the knee joint and surgical interventions in this region of the bone.

2. Material and method

The research was carried out in several stages, i.e. experimental studies – to determine the distribution of tibial bone loads and acquire data for the validation of FEM models, numerical studies conducted on three-dimensional models – to determine the strain pattern in bone tissue in detail and numerical simulations using two-dimensional FEM models – to trace the adaptations in bone tissue.

The experimental studies covered the analysis of the pattern of tibial bone displacements in the frontal and sagittal planes by means of the holographic interferometry method. The studies were conducted on physical models of a healthy knee joint, a deformed knee joint and a knee joint after a surgical operation.

The numerical three-dimensional model studies were conducted with the application of the finite element method. Models of tibial bone and fibula connected in a complex of shank bones by soft tissues were developed. The models were subjected to loading same as when standing on one leg. The bone tissue strain patterns in models of healthy tibial bone, deformed (varus deformity), after "plus" and "minus" popliteal osteotomy and after knee joint alloplasty tibial bone were determined.

The same numerical studies were carried out on two-dimensional models. The load to which the tibial bone models were subjected was calculated for the support stage in walking. Simulations were run for the same conditions as in the case of the three-dimensional models. Computer software Ansys 5.6 was used for the computations.

2.1. Experimental studies

First basic relationships in the knee joint biomechanics, such as the way in which loads are carried by the elements of the joint and how they are distributed in them (particularly in the skeletal system elements) and the displacements of knee joint bones for different joint configurations and selected states of loading, were determined.

A holographic interferometry analysis of the state of displacements included the research of knee joint physical models for the following configurations: the healthy condition, the varus deformity condition and the condition after popliteal osteotomy. In all the cases the research was conducted on knee joint models consisting of the distal epiphysis of femur bone and the proximal epiphysis of tibial bone. Both epiphyses were parts of real bones dissected free from cadavers (Fig. 1). The models were subjected to loading with an axial force applied in the system shown in Fig. 2a.

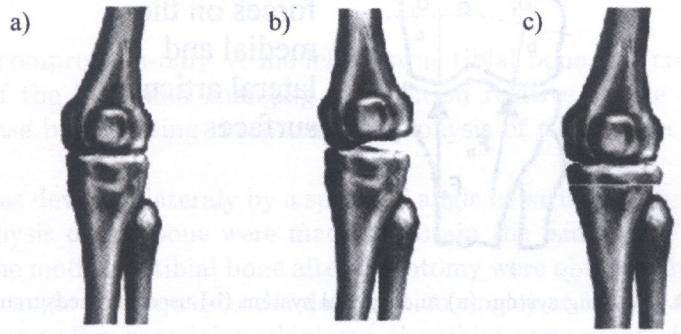

Fig. 1. Stages of experimental studies and corresponding models of a) model of healthy joint, b) model of varus joint, c) model of a joint after high tibial osteotomy

Detailed load values are given in Table 1. Double exposure technique was used. Measurement system is shown in Fig. 2b. The recorded interferograms were examined and the distribution of

Table 1. Loading force values in all four stages of loading

	Joint loading force [N]	Increment in force [N]
Stage 1	170	5
	230	5
Stage 2	170	5
	230	5
Stage 3	170	5
	230	5

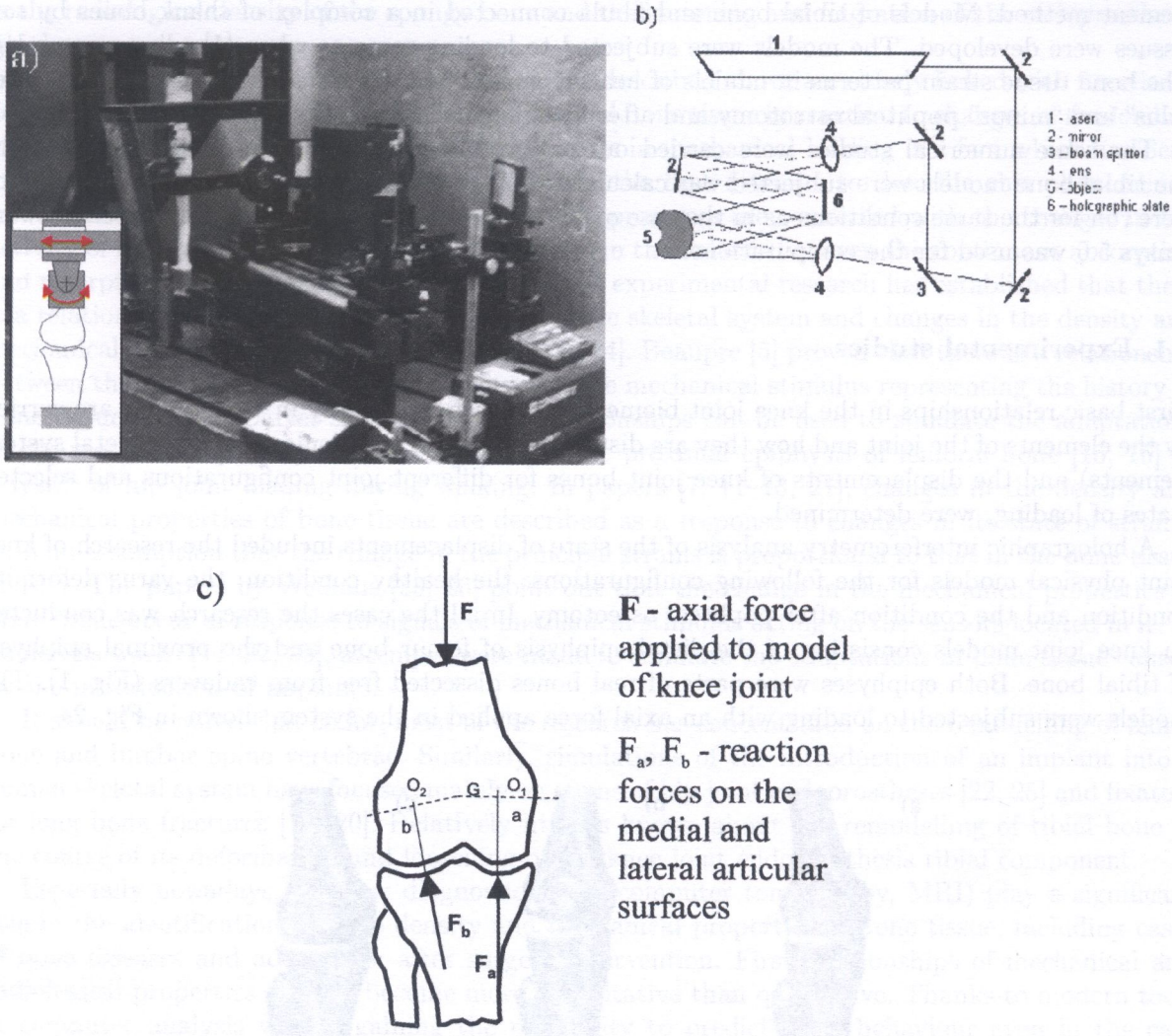

Fig. 2. Loading system (a) and optical system (b) used for measurements

displacements in the sagittal plane along a line running vertically through the geometrical centre of the joint was determined.

2.2. Numerical studies conducted on three-dimensional models

The principal aim at this stage was to determine the relationship between the external load (in this case acting on the knee joint) and the state of strains in the bone tissue.

Computations were performed using three-dimensional tibial bone models developed on the basis of physical models of the bone (Sawbones) [28]. The outer surface of tibial bone models was measured by scanning the coordinates of points by means of a three-dimensional scanner (Digiboot). The inner surface of compact bone was obtained through the analysis of computer tomograms obtained by x-raying the same physical models of the bone. A solid element with 12 nodes and three degrees of freedom in each node was used to form a finite element mesh (Fig. 3).

A tension link-type elements with two nodes and three degrees of freedom in each node were used to model soft tissues. Only soft tissues connecting tibia and fibula bone were modelled (interosseous membrane, tibio-fibular syndesmosis). Elements used by option tension-only were used for modelling of interosseous membrane. In the modelling of both syndesmosis only the elements by option tension

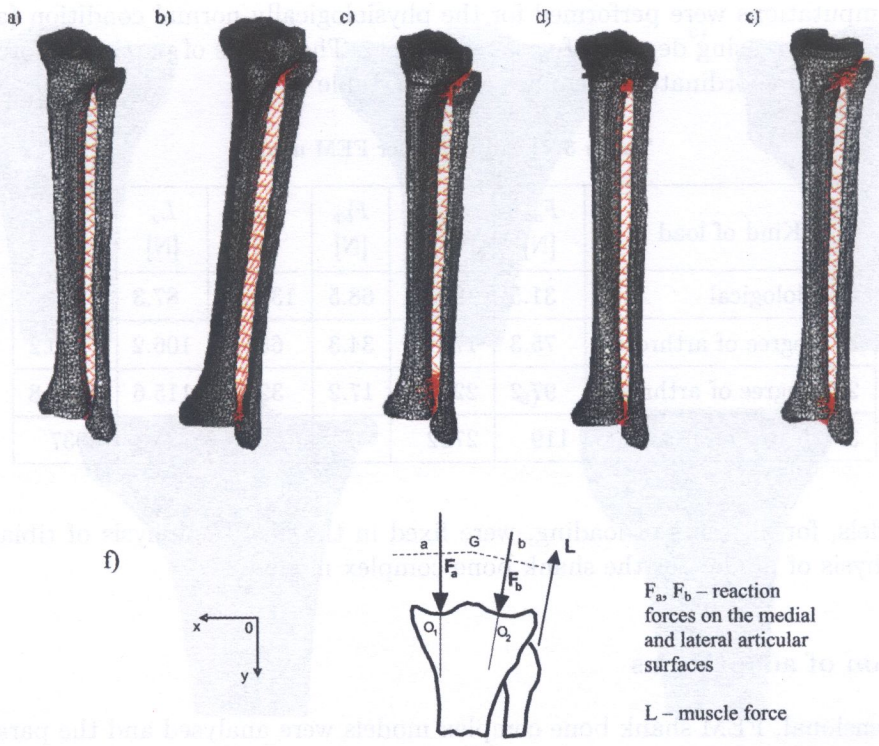

Fig. 3. FEM model of the complex of shank bones: (a) healthy, (b) varus, (c) after plus osteotomy, (d) after minus osteotomy and (e) after knee joint alloplasty (f) loading model

were used as well as compression-only. A model of varus tibial bone was created by deforming the proximal epiphysis of the bone and changing its position relative to the mechanical axis of the lower limb (in this case by deviating the proximal epiphysis of tibial bone lateraly from its distal epiphysis).

The bone model was deviated lateraly by a specified angle of varus deformity and then alterations in the proximal epiphysis of the bone were made to obtain the "sinking-in" of the medial condyle under overloading. The models of tibial bone after osteotomy were obtained by inserting or removing a wedge (whose apex angle was equal to the deformation angle) at half of the internodal segment. In the model of the bone after knee joint alloplasty, the tibial component of a knee joint prosthesis (Search) fixed with bone cement was reproduced. The material properties of all the tissues occurring in the models are given in Table 2. All model materials were represented as linear-elastic.

Table 2. Material properties of model tissues

Kind of tissue	Modulus of elasticity E [MPa]	Poisson's ratio ν
Compact bone	18600	0.3
Spongy bone	450	0.42
Tibiofibular syndesmosis (option: only tension)	2500	–
Tibiofibular syndesmosis (option: only compression)	3500	–
Interosseous membrane	860	–

Situations of asymmetrical standing on one lower limb were simulated. The Maquet model [18] was used to determine the loads acting on a knee joint. The latter were calculated for a body mass of

72 kg. First computations were performed for the physiologically normal condition (a healthy knee joint) and then for increasing degrees of varus deformity. The values of particular force components in the assumed global coordinate system are given in Table 3.

Table 3. Load values for FEM models

Kind of load	F_{ax} [N]	F_{ay} [N]	F_{bx} [N]	F_{by} [N]	L_x [N]	L_y [N]
Physiological	31.5	801	68.5	1303.8	87.3	1423
1st degree of arthrosis	75.3	1761.9	34.3	651.9	106.2	1730.2
2nd degree of arthrosis	97.2	2242.3	17.2	326	115.6	1883.8
3rd degree of arthrosis	119	2722	0	0	125	2037

All the models, for all cases of loading, were fixed in the distal epiphysis of tibial bone and in the distal epiphysis of fibula (for the shank bone complex model).

2.3. Simulation of adaptations

The three-dimensional, FEM shank bone complex models were analysed and the parameters of the state of stress and strain characteristic for a healthy joint model, the deformed joint model and the model of the joint after the most common (for this region of the joint) surgical procedures were determined. However, the obtained results did not make it possible to trace either the course of the joint deformation or that of the remodelling of the normal bone structure after corrective procedures. Therefore a decision was made to simulate the change in the properties of bone tissue by a change in loading (due to the increasing deformation of the lower limb or a surgical treatment).

The functional adaptation of bone tissue was also simulated by means of FEM models (Fig. 4). Data on the geometry of the models and their loading were taken from the three-dimensional model computations. Two-dimensional quadrilateral elements, each with eight nodes and two degrees of freedom, were used to create a FE mesh.

The models were used for the simulation of bone tissue adaptations according to the following algorithm:

1. compute the state of stress and strain for all the model loading cases;
2. compute the effective stress for each finite element in the model according to this relation:

$$\sigma_i = \sqrt{2EU}, \tag{1}$$

where E – Young's modulus for a given element; U – an elastic strain energy value;

3. compute the distribution of the mechanical, remodelling stimulus from this relation [15]:

$$\varphi = \left(\sum_{i=1}^{N} n_i \sqrt[m]{\sigma_i} \right)^m, \tag{2}$$

where i – another case of loading; n – a number of cycles for the i-th case of loading; m – an experimentally determined coefficient;

4. compute the change in bone tissue density for each finite element according to the linear model of functional adaptation; the model assumes a certain value of the mechanical stimulus corresponding to the state of equilibrium of bone tissue absorption and resorption; it is also assumed

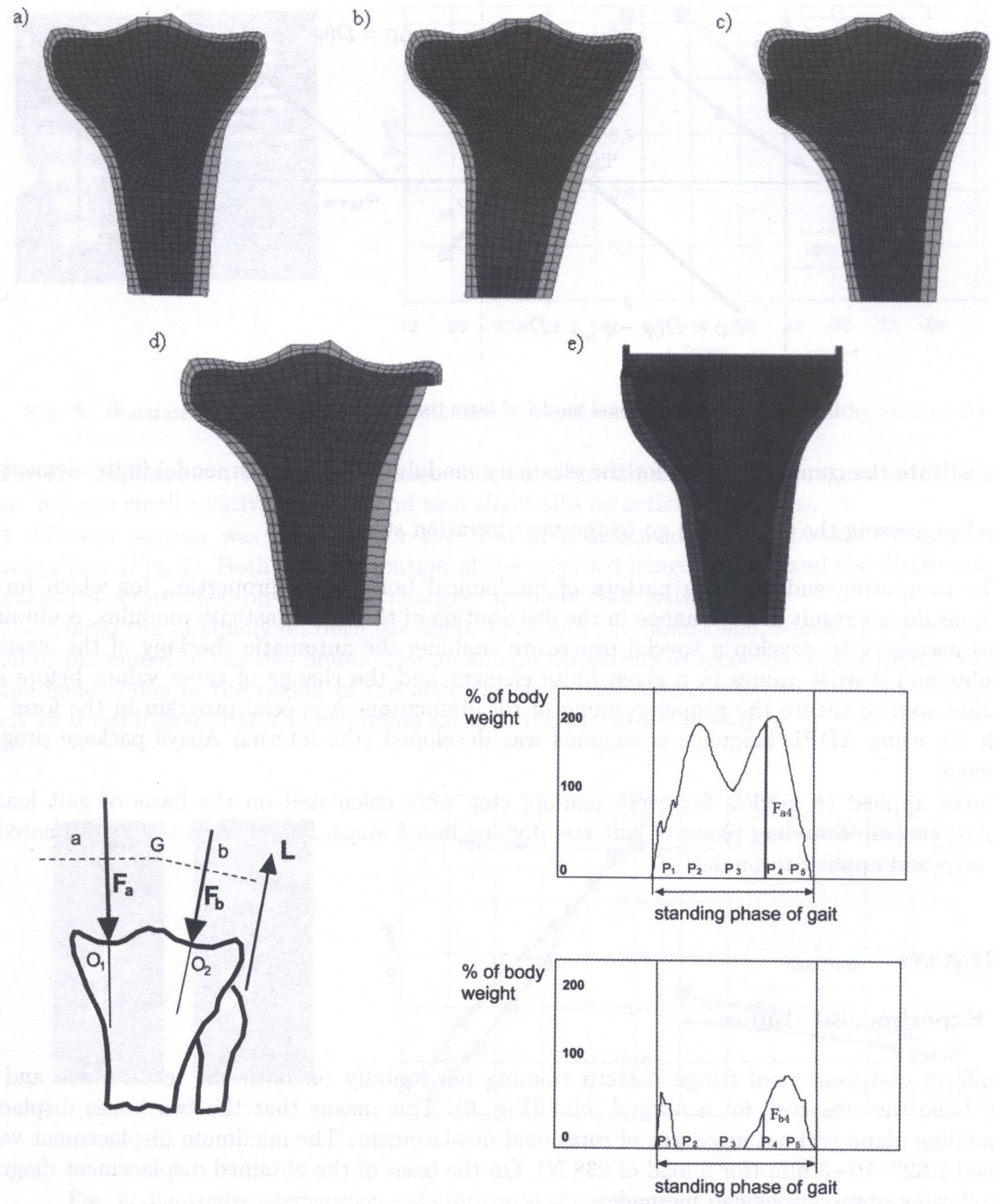

Fig. 4. FEM models used for adaptation simulation: healthy bone model (a), varus bone model (b), post-osteotomy bone model (c), (d) and post-alloplasty bone model (e) loading model for remodelling simulation (f)

that if a mechanical stimulus value, within a certain interval above and below the value corresponding to the state of equilibrium, is generated, no change will occur; only if the limits of this interval are exceeded, bone tissue absorption or resorption will result; with bone density change, the value being proportional to the mechanical stimulus value (Fig. 5);

5. compute the change in the modulus of elasticity for each finite element in the model according to this relation [9]:

$$E = A\rho^B, \tag{3}$$

where ρ – a bone tissue density value; A, B – experimentally determined coefficients;

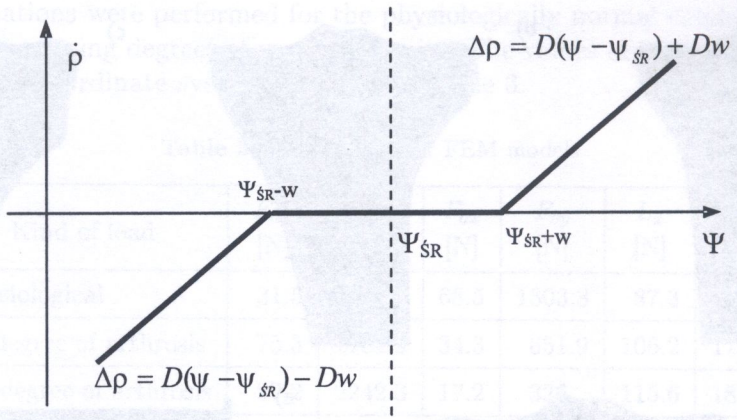

Fig. 5. Computational model of bone tissue functional adaptation

6. substitute the computed value for the elasticity modulus value in each model finite element;

7. end processing the model and go to the next iteration step.

The computing ends when a pattern of mechanical bone tissue properties, for which further iterations do not result in any change in the distribution of the bone elasticity modulus, is obtained. It was necessary to develop a special procedure enabling the automatic checking of the elasticity modulus and density values in a given finite element and the change of these values before each iteration step to ensure the proper running of the simulation. A special program in the form of a batch file using ADPL language commands was developed (the internal Ansys package program language).

Forces applied to models for every loading step were calculated on the basis of gait loading calculations [13]. Standing phase of gait was divided into 5 steps. Forces' values were estimated for each step and applied to model.

3. Results

3.1. Experimental studies

A uniform distribution of fringe pattern running horizontally on both the femur bone and the tibial bone was observed for a normal joint (Fig. 6). This means that the two bones displace in the midline plane without any signs of rotational displacement. The maximum displacement values reached $2.827 \cdot 10{-}3$ mm (for a load of 238 N). On the basis of the obtained displacement diagrams the following observations can be made:

1. the tibial bone, rigidly fixed at its distal part, is simultaneously compressed and bent under the action of the femur bone; its proximal epiphysis displaces backwards but the displacement values are low ($1.542 \cdot 10^{-3}$ mm);

2. the femur bone displaces as a rigid solid under the applied load and, due to the reactions on articular surfaces, shifts forward; the femur bone was fixed in the proximal part in a way which made its parallel shift in the sagittal plane and rotation around a fixed rotation axis located on the weighing lever possible; in consequence of this fixation the femur bone acquired as many degrees of freedom as in a real joint; the distribution of displacements shows that the bone has shifted forward and rotated slightly in the midline plane; in this case the maximum displacement values are low ($2.827 \cdot 10^{-3}$ mm).

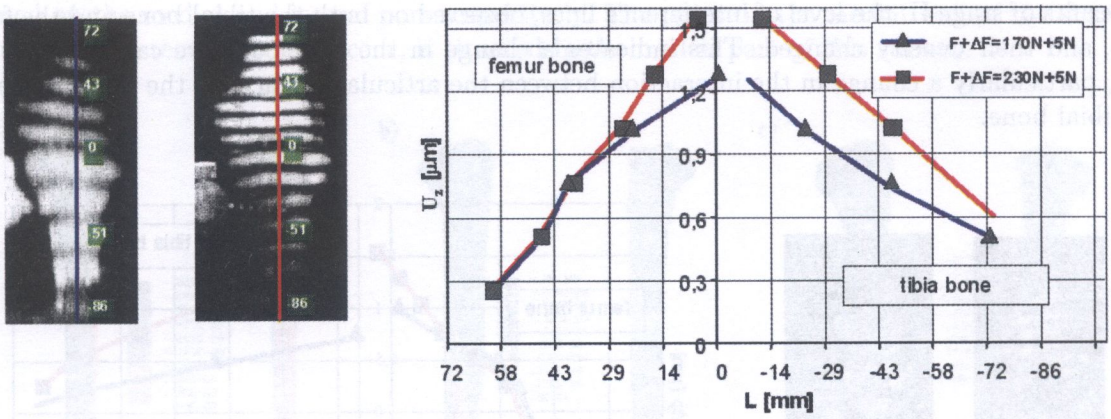

Fig. 6. Illustrative interferogram and distribution of displacements recorded for a healthy joint model

The low displacement values on the femur bone and the tibial bone in the region of the articular space indicate small relative motions and so a slight slip on articular surfaces.

A different pattern was observed for the joint of a deformed limb – the second stage of the investigations (Fig. 7). Both the distribution of the recorded fringe pattern and the distributions of displacement determined on this basis changed in comparison with stage I.

The fringes run obliquely on both the femur bone and the tibial bone, which indicates the rotational displacement of the two bones. The maximum displacement recorded on the model occurred on the femur bone in the region of the articular space and it amounted to $3.88 \cdot 10^{-2}$ mm. It is about 15 times higher than the maximum displacement recorded in stage I.

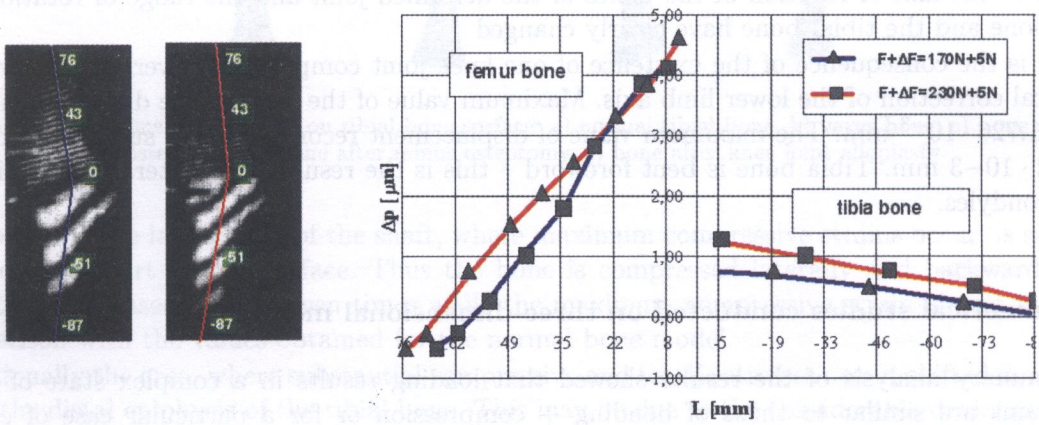

Fig. 7. Illustrative interferogram and distribution of displacements recorded for a varus joint

In this case the femur bone displaced as a rigid solid, which for the support on only one condyle resulted in considerable rotation around the axis running through the medial condyle of the knee joint. The tibial bone was loaded by a force passing through the articular surfaces of the medial condyle. The obtained pattern of fringes resulted from bending in the frontal and sagittal plane and torsion of the tibial bone around the vertical axis. The tibial bone was rigidly fixed so the maximum displacement values on the proximal epiphysis are much lower than those observed on the femur bone. The mutual displacements of the articular surfaces (here they can be regarded as a slip) increased considerably in comparison with stage I.

Stage III included studies of the displacements of the joint after the correction of the mechanical axis according to the Coventry method. The obtained results show a significant effect of the surgical correction on the pattern of interference lines and on displacements (Fig. 8). In comparison with

the results of stage II, the level of interference lines, observed on both the tibial bone and the femur bone, and their density changed. This indicates a change in the way loads are carried by a knee joint, particularly a change in the interaction between the articular surfaces of the femur bone and the tibial bone.

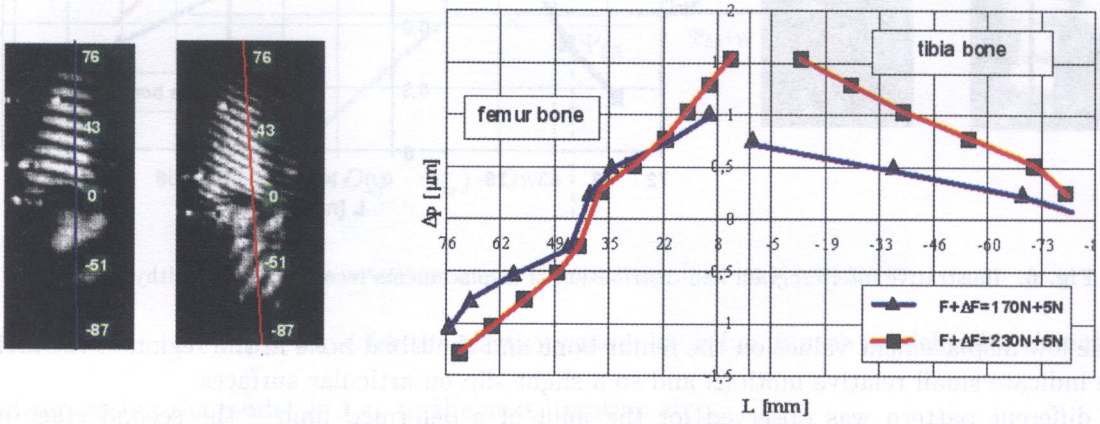

Fig. 8. Illustrative interferogram and distribution of displacements recorded for a joint after popliteal osteotomy

Owing to the correction of the axis in the model, better contact between the articular surfaces on both the medial part and the lateral part was obtained. Nevertheless, the pattern of fringes indicates that the axis of rotation of the femur bone still runs on the medial part but its position in relation to the axis of rotation of the bones of the deformed joint and the range of rotation of the femur bone and the tibial bone have clearly changed.

This is the consequence of the existence of one knee joint compartment overloading, even after a surgical correction of the lower limb axis. Maximum value of the femur bone displacement in this case is $1.726 \cdot 10^{-3}$ mm. The maximum value of displacement recorded on the surface of tibia bone is $1.542 \cdot 10{-}3$ mm. Tibia bone is bent foreword – this is the result of the interaction of tibia and femur condyles.

3.2. Numerical studies conducted on three-dimensional models

A preliminary analysis of the results showed that loading results in a complex state of stresses and strains are similar to those of bending + compression or for a particular case of eccentric compression. The bone bending effect is significantly smaller than for the femur bone bending but it is still noticeable, particularly in the shaft region. The state of strains in the shank bone complex was analysed for all the above mentioned bone models, i.e. the normal tibial bone, the varus bone, the bone after plus and minus osteotomy and the bone after knee joint alloplasty. The distribution of strains ε_z (along the vertical axis coinciding with the longitudinal axis of the tibial bone) was analysed for all models. The highest values of ε_z were obtained on lateral surfaces of the bone shaft in its distal part (Fig. 9). The recorded strain distributions on bone surface indicate changes in the global state of strains of the whole tibial bone resulting from its loading and position. In the case of the normal bone (whose anatomical axis is vertical) one can observe a concentration of compressive strains on the medial-posterior part and a concentration of tensile strains on the lateral-anterior part. The tibial bone is bent towards the medial part and backwards. The effect of the forward displacement of the tibial bone under loading was also obtained in the experimental studies. It is characteristic that the maximum compressive strain on the medial part is twice as high as the maximum tensile stress on the lateral part. For the varus bone, tensile and compressive strains are

observed on the medial and lateral part respectively. The point on the medial wall of the shaft, at which maximum tensile strains occur, is situated in the medial part of this surface.

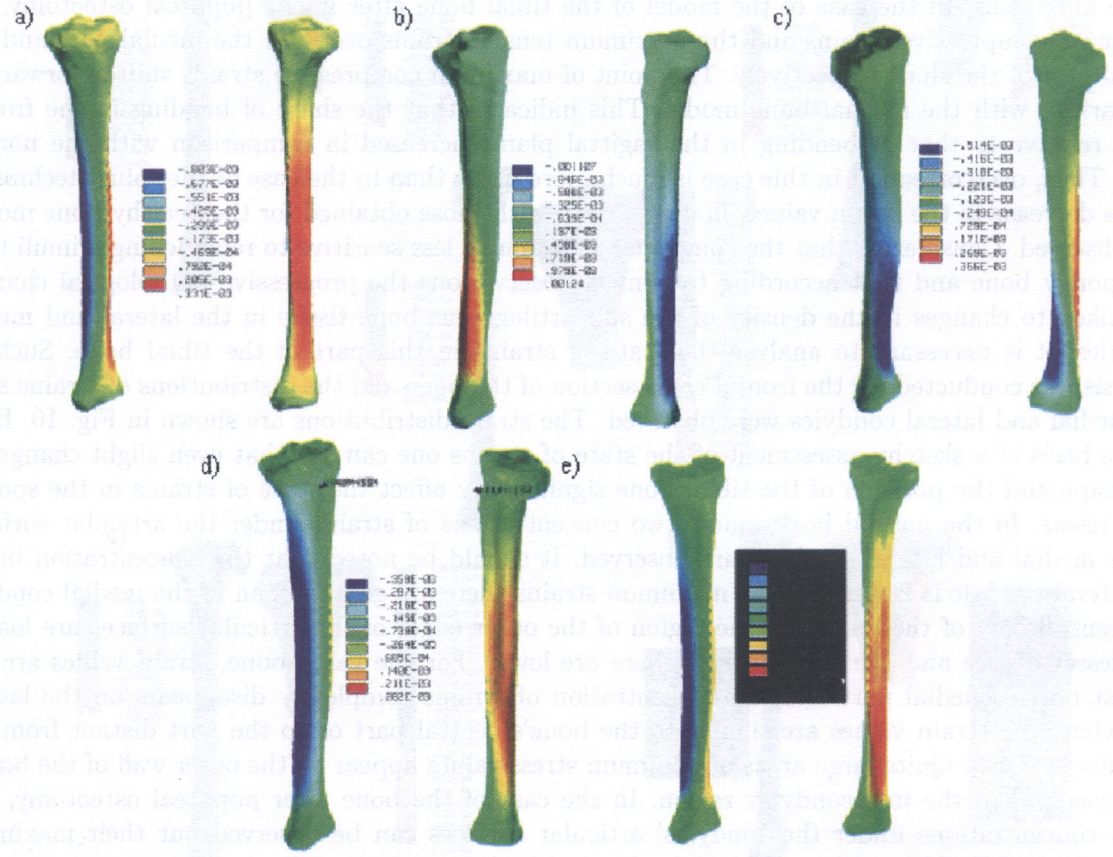

Fig. 9. Distributions of strains εz on tibial bone surface: a) normal tibial bone, b) varus bone, c) bone after plus osteotomy, d) bone after minus osteotomy, e) bone after knee joint alloplasty

The point on the lateral wall of the shaft, where maximum compressive strains occur, is situated in the posterior part of this surface. Thus the bone is compressed laterally and backwards. The tensile strain increased nearly seven times while the maximum compressive strain almost doubled, in comparison with the values obtained for the normal bone model.

Additionally the area, where substantial compressive and tensile stresses occur, shifted downward towards the distal epiphysis of the tibial bone. This may be due to the considerable deviation of the tibial bone from the lower limb's mechanical axis to the side. In the case of the post-plus-osteotomy bone model, the maximum compressive stresses occur on the anterior side of the bone shaft's medial wall and in the distal part they can be observed even on the anterior edge of the shaft. The maximum tensile stresses occur on the posterior part of the side wall and near the epiphysis – on the back wall. This indicates that the bone is strongly bent in the coronal plane and this effect dominates over bending in the sagittal plane. This is corroborated by the fact that the maximum compressive strains decreased in comparison with the healthy bone and the tensile strains remained at a similar level.

Thus the state of strains characteristic of the normal bone model was not obtained in this case, even though a proper corrective procedure was applied. Changes in the shape of the proximal epiphysis of the bone resulted in a different way of carrying loads, particularly on the medial part of the bone's epiphysis.

A rigid wedge (of considerable thickness) on the medial part (correction 12°) resulted in a significant reduction in the tendency of the bone's epiphysis towards displacement to the medial side

relative to the shaft. Thus one can say that in the case of the correction of the axis by plus popliteal osteotomy, the risk that a too small wedge will be used and the so called "hypercorrection" will result is relatively slight. The use of a too large bone wedge can lead to the return of the varus deformity of the knee joint. In the case of the model of the tibial bone after minus popliteal osteotomy, the maximum compressive strains and the maximum tensile strains occur on the medial part and the lateral part of the shaft respectively. The point of maximum compressive strains shifted forward in comparison with the normal bone model. This indicates that the share of bending in the frontal plane relative to that of bending in the sagittal plane increased in comparison with the normal bone. Thus, overcorrection in this case is much more likely than in the case of the "plus" technique. Also a decrease in the strain values, in comparison with those obtained for the healthy bone model, was observed. Considering that the compact bone is much less sensitive to remodelling stimuli than the spongy bone and that according to clinical observations the progressive pathological changes are linked to changes in the density of the subcartilaginous bone tissue in the lateral and medial condyles, it is necessary to analyse the state of strains in this part of the tibial bone. Such an analysis was conducted for the frontal cross-section of the bone and the distributions of strains ε_z in the medial and lateral condyles were observed. The strain distributions are shown in Fig. 10. Even on the basis of a sketchy assessment of the state of strains one can say that even slight changes in the shape and the position of the tibial bone significantly affect the state of strains in the spongy bone tissue. In the normal bone model two concentrations of strains under the articular surfaces of the medial and lateral condyles are observed. It should be noted that the concentration under the lateral condyle is larger and the maximum strains there are greater than in the medial condyle. The central part of the bone and the region of the outer edges of the articular surfaces are loaded to a lesser degree and the strain values there are lower. For the varus bone, strain values are the highest on the medial part and the concentration of strains completely disappears on the lateral side where the strain values are similar to the bone's central part or to the part distant from the articular surfaces. Quite large areas of minimum stress values appear on the outer wall of the bone's epiphysis and in the intercondylar region. In the case of the bone after popliteal osteotomy, two strain concentrations under the condyles' articular surfaces can be observed but their maximum strain values differ from those observed in the healthy bone model.

For the plus popliteal osteotomy the concentration of strains in the subcartilaginous layer of the lateral condyle is larger than in the medial condyle but a decrease in the maximum strain values in both condyles in comparison with the ones obtained for the normal bone model is observed. A different picture emerges in the case of minus popliteal osteotomy: a larger concentration of strains occurs on the medial part. Thus, although the varus deformity effect has been corrected to a considerable degree, the medial condyle is still somewhat overloaded while the lateral condyle is slightly underloaded. In addition, concentrations of tensile strains, due to the separation of the upper fragment of the bone from the connecting surface caused by the action of the muscular force directed upward on the lateral side, occur in the spongy bone in the region of the rapid change in the epiphysis cross-section, resulting from the resection of the bone wedge.

In reality, such concentrations of strains will appear only at a certain stage of synostosis when a permanent union between the bone fragments is formed. Hence one can infer that bone remodelling and union on the lateral part of the bone will be hampered due to unphysiological state of strains in the bone tissue. The maximum compressive strain values in the subcartilagionus layer are lower than the ones observed in the normal bone model.

In the post-alloplasty bone model, compressive strain concentrations were observed under the prosthesis condylar plate's surface and at the end of the stem of the prosthesis tibial component. Also in the region of the contact between the prosthesis plate and the cortical bone tissue one can notice a considerable increase in the strains in the bone due to the direct action of the metallic implant on the bone tissue. The strain values in the two articular compartments are similar but they are higher than in the normal bone model. In addition, the concentration of substantial strains which occurs at the end of the condyle may contribute to the remodelling of the bone tissue.

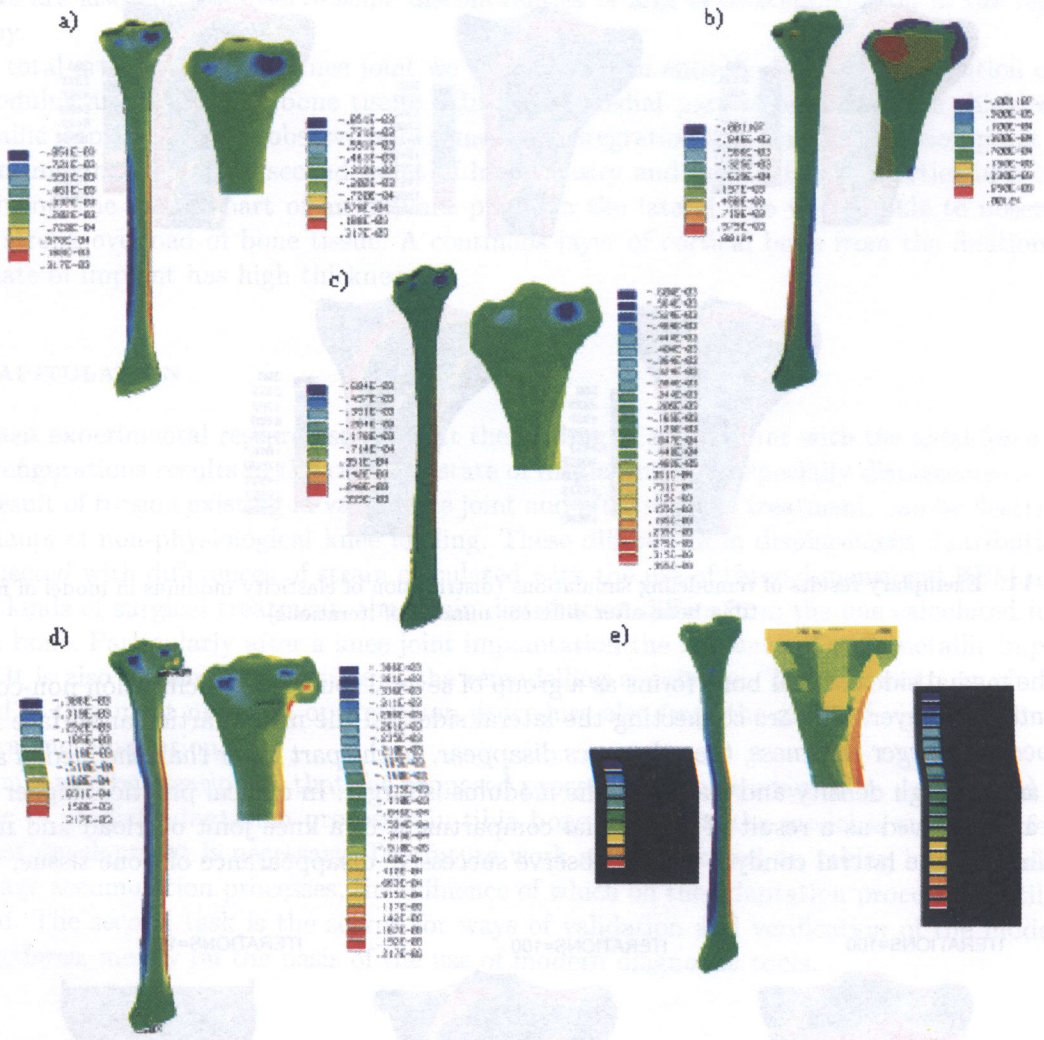

Fig. 10. Distributions of strains εz in the frontal plane of the tibial bone: a) normal tibial bone, b) varus bone, c) bone after plus osteotomy, d) bone after minus osteotomy, e) bone after knee joint alloplasty

3.3. Simulations of bone tissue adaptations

Simulations of bone remodelling were conducted with the use of two-dimensional FEM models. In the model of proper tibia bone, the remodelling of bone tissue starts rapidly after several iterations in the region of the lateral edge of a bone model. A cortical bone layer starts forming from the fixation point up to the region of articular surfaces. In the medial side of bone it is possible to observe some points in which cortical bone tissue starts forming, but the continuous layer does not appear just like on the lateral side (Fig. 11).

Visible parts of bone with high density and mechanical properties are perceivable also in the region of a medial articular surface and an intracondylar part of bone. Some parts of bone tissue on the lines (arcs), connecting fixation points on the lateral side and medial articular surface, also have higher density and stiffness values. In numerous clinical observations and references in literature the presence of this kind of arcs formed by bone tissue trabeculaes is confirmed.

The simulation realized with the use varus bone model showed that the change of shape and load of the articular surfaces results in a completely different distribution of density and elasticity modulus of bone tissue. The impact of bone tissue layer on the lateral side of bone intensifies, the new layer has higher thickness, but its upper end is located lower, accordingly to the model of a normal bone. It is the result of a decrease in bone tissue properties in all lateral condyle.

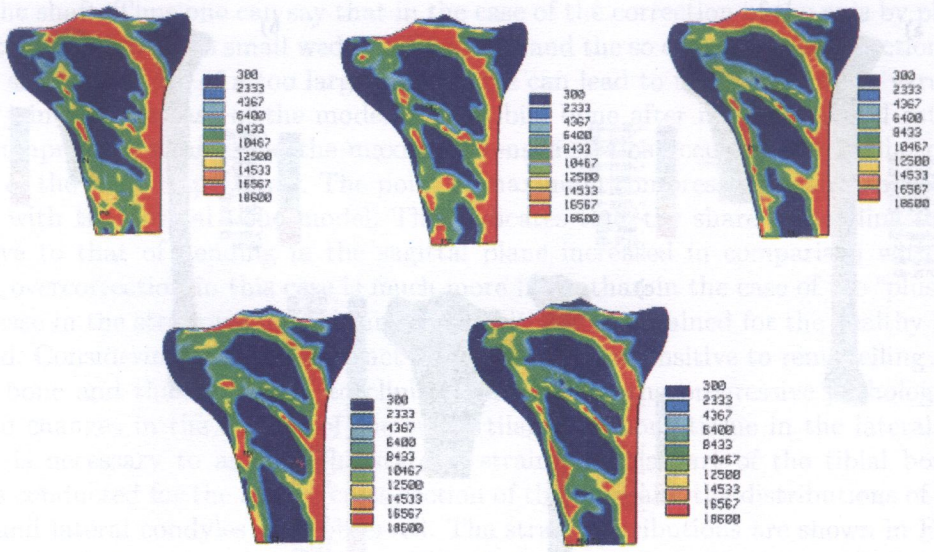

Fig. 11. Exemplary results of remodeling simulations (distribution of elasticity modulus in model of normal tibia bone after different number of iterations)

In the medial side cortical bone forms as a group of several sources of calcification non-connected in a continuous layer. The arc connecting the lateral side and the medial articular surface is better developed, has larger thickness, the other arcs disappear. In the part lower than the medial articular surface area of high density and elasticity, the modulus is larger. In clinical practice, higher density regions are observed as a result of the medial compartment of a knee joint overload and intensive remodeling. In the lateral condyle we can observe successive disappearance of bone tissue.

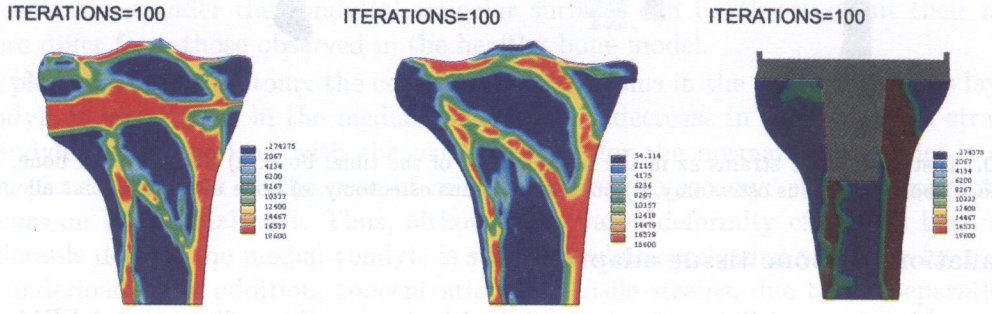

Fig. 12. Exemplary results of remodeling simulations (distribution of elasticity modulus in model of varus and treated tibia bone after 100 iterations)

Following the correction using high tibial osteotomy ("plus" technique) we can observe that the layer of cortical bone tissue on the lateral side is almost the same size as in the normal bone model (Fig. 12). In the medial size we can still observe several sources of osteointegration, but in the upper region (above the wedge) it becomes more developed especially in the region of the upper medial corner of the model (in that area the bone was not well developed in the model of a normal bone). Arcs connecting medial and lateral sides of bone mostly disappear, only one arc connects the medial and the lateral side of the model. In the upper part we can observe the development of two new arcs connecting wedge and articular surfaces. Especially in the lateral part of medial condyle, it starts to form a large area of osteointegration. Also after the correction with the application of popliteal osteotomy ("minus" technique) the layer of cortical bone tissue on the lateral side is similar. We can observe some disturbances in osteointegration process in the region of the removed wedge in the lateral side of a bone. The bone is characterized by a higher value of elasticity modulus in this

region, we are also able to observe some discontinuities of arcs of osteointegration in the region of osteotomy.

After total arthroplasty of a knee joint we can observe an entirely different distribution of elasticity modulus and density of bone tissue. Almost all medial part of bone is stress shielded by a stiff metallic implant. We can observe only some osteointegration line from the fixation point to the end of an implant stem. The second point of high density and mechanical properties in a bone is located below the medial part of an implant plate. In the lateral side we are able to observe the effect of strong overload of bone tissue. A continuos layer of cortical bone from the fixation point to the plate of implant has high thickness.

4. Recapitulation

The present experimental research shows that the loading of a knee joint with the axial force in different configurations results in the complex state of displacements. Especially displacements, which are the result of torsion existing in varus knee joint and after surgical treatment, can be described as determinants of non-physiological knee loading. These differences in displacement distribution are also connected with differences of strain calculated with the use of three-dimensional FEM models. After all kinds of surgical treatment, the strain distribution differs from the one calculated for normal tibia bone. Particularly after a knee joint implantation the influence of stiff, metallic implant is distinct. It is also visible in the results of the remodelling simulation. This allows to conclude that each kind of treatment needs an optimisation procedure also from the point of view of bone tissue mechanics and adaptation.

It should also be mentioned, that the proposed procedure of bone adaptation was applied for the first time to predict adaptation processes in tibia bone. However, the model is still imperfect and its further development is necessary. The future work will be focused on taking into consideration the damage accumulation processes, the influence of which on the adaptation processes is still being discussed. The second task is the search for ways of validation and verification of the models and the procedures, mostly on the basis of the use of modern diagnostic tools.

Acknowledgments

This work was supported by Polish State Committee for Scientific Research: Grant No. 5 T07A 028 23.

References

[1] R. Będziński, K. Ścigała, M. Bernakiewicz. Biomechanical aspects of artificial joint implantation in a lower limb. *Journal of Applied and Theoretical Mechanics*, **37**: 455–479, 1999.

[2] R. Będziński. *Biomechanika inżynierska. Zagadnienia wybrane* (in Polish). Wydawnictwo Politechniki Wrocławskiej, Wrocław, 1997.

[3] R. Będziński, A. Pozowski, K. Ścigała. Experimental verification of tibial osteotomy performed using different techniques. *Procc. 19th Danubia Adria Symposium on Experimental Methods in Solid Mechanics*. 41–44, Slovakia, 1996.

[4] R. Będziński, K. Ścigała. Experimental analysis of surgically corrected knee joint. *Strain*, **34**: 188–194, 1998.

[5] G. S. Beaupre, T. E. Orr, D. R. Carter. An approach for time – dependent bone modeling and remodeling applications: a preliminary simulation. *Journal Orthop. Res.* **8**: 662–670, 1990.

[6] D. B. Burr, R. B. Martin, M. B. Schaffer, E. L. Randin. Bone remodeling in response to in vivo fatigue microdamege. *J. Biomechanics*, **18**: 189–200, 1985.

[7] D. R. Carter. Mechanical loading history and skeletal biology. *J. Biomechanics*, **20**: 1095–1109, 1987.

[8] D. R. Carter, D. P. Fyhrie, R. T. Whalen. Trabecular bone density and loading history: regulation of connective tissue biology by mechanical energy. *J. Biomechanics*, **20**: 785–794, 1987.

[9] D. R. Carter, W. C. Hayes. The compressive behavior of bone as a two-phase porous structure. *Journal of Bone and Joint Surgery*, **59A**: 954–962, 1977.

[10] E. J. Cheal, W. C. Hayes, A. A. White. Stress analysis of compression plate fixation and its effects on long bone remodeling. *J. Biomechanics*, **18**: 141–150, 1985.
[11] E. Y. S. Chao. A survey of finite element analysis in orthopedic biomechanics: the first decade. R. Huiskes. *J. Biomechanics*, **16**: 385–409, 1983.
[12] S. C. Cowin, R. T. Hart, J. R. Balser, D. H. Kohn. Functional adaptation in long bones: establishing in vivo values for surface remodeling rate coefficients. *J. Biomechanics*, **18**: 665–684, 1985.
[13] D. E. Hurwitz, D. R. Summer, T. P. Andriacchi, D. A. Sugar. Dynamic knee loads during gait predict tibial bone distribution. *Journal of Biomechanics*, **31**: 423–430, 1998.
[14] R. Huiskes, H. Weinans, H. J. Grootenboer, M. Dalstra, B. Fundala, T. J. Slooff. Adaptive bone-remodelling theory applied to prosthetic design analysis. *Journal of Biomechanics*, **20**: 1135–1150, 1987.
[15] C. R. Jacobs, J. C. Simo, G. S. Beaupre, D. R. Carter. Adaptive bone remodeling incorporating simultaneous density and anisotropy considerations. *Journal of Biomechanics*, **30**: 603–613, 1997.
[16] C. R. Jacobs, M. E. Levenston, G. S. Beaupre, J. C. Simo, D. R. Carter. Numerical instabilities in bone remodeling simulations: the advantages of a node-based finite element approach. *Journal of Biomechanics*, **28**: 449–459, 1995.
[17] L. E. Lanyon. Functional strain in bone tissue as an objective, and controlling stimulus for adaptive bone remodeling. *Journal of Biomechanics*, **20**: 1083–1093, 1987.
[18] P. G. Maquet. *Biomechanics of knee*, Springer-Verlag, Berlin, 1983.
[19] G. Marotti, M. Ferretti, M. A. Muglia, C. Palumbo, Palazzini. A quantitative evaluation of osteoblast-osteocyte relationships on growing endosteal surface of rabbit tibiae, S., *Bone*, **13**: 363–368, 1992.
[20] D. M. O'Doherty, S. P. Butler, A. E. Goodship. Stress protection due to external fixation. *Journal of Biomechanics*, **28**: 575–586, 1995.
[21] P. J. Prendergast. Finite Element Models in tissue mechanics and orthopaedic implant design. *Clinical Biomechanics*, **12**: 343–366, 1997.
[22] B. van Rietbergen, R. Huiskes, H. Weinans, D. R. Sumner, T. M. Turner, J. O. Galante. The mechanism of bone remodeling and resorption around press-fitted THA stems. *Journal of Biomechanics*, **26**: 369–382, 1993.
[23] B. van Rietbergen, H. Weinans, R. Huiskes, A. Odgaard. A new method to determine trabecular bone elastic properties and loading using micromechanical finite-element models. *Journal of Biomechanics*, **28**: 69–81, 1995.
[24] C. H. Turner, V. Anne, R. M. Pidaparti. A unifrom strain criterion for trabecular bone adaptation: do continuum-level strain gradients drive adaptation. *Journal of Biomechanics*, **30**: 555–564, 1997.
[25] D. R. Turner, T. M. Igloria, R. M. Urban, J. O. Galante. Functional adaptation and ingrowth of bone vary as a function of hip implant stiffness. *Journal of Biomechanics*, **31**: 909–917, 1998.
[26] H. Weinans, R. Huiskes, H. J. Grootenboer. The behavior of adaptive bone-remodeling simulation models. *Journal of Biomechanics*, **25**: 1425–1441, 1992.
[27] J. Wolff. *Ueber die Bedeutung der Architectur der spongiosen Substanz fur die Frange vom Knochenwachsthum.* Zentralblatt fur die Medizinischen Wissenschaften, 1869.
[28] http://www.sawbones.se